

Esco2 Regulates *cx43* Expression During Skeletal Regeneration in the Zebrafish Fin

Rajeswari Banerji, Diane M. Eble, M. Kathryn Iovine,* and Robert V. Skibbens*

Department of Biological Science, Lehigh University, Bethlehem, Pennsylvania

Background: Roberts syndrome (RBS) is a rare genetic disorder characterized by craniofacial abnormalities, limb malformation, and often severe mental retardation. RBS arises from mutations in *ESCO2* that encodes an acetyltransferase and modifies the cohesin subunit *SMC3*. Mutations in *SCC2/NIPBL* (encodes a cohesin loader), *SMC3* or other cohesin genes (*SMC1*, *RAD21/MCD1*) give rise to a related developmental malady termed Cornelia de Lange syndrome (CdLS). RBS and CdLS exhibit overlapping phenotypes, but RBS is thought to arise through mitotic failure and limited progenitor cell proliferation while CdLS arises through transcriptional dysregulation. Here, we use the zebrafish regenerating fin model to test the mechanism through which RBS-type phenotypes arise. **Results:** *esco2* is up-regulated during fin regeneration and specifically within the blastema. *esco2* knockdown adversely affects both tissue and bone growth in regenerating fins—consistent with a role in skeletal morphogenesis. *esco2*-knockdown significantly diminishes *cx43/gja1* expression which encodes the gap junction connexin subunit required for cell–cell communication. *cx43* mutations cause the *short fin (sof^{b123})* phenotype in zebrafish and oculodentodigital dysplasia (ODDD) in humans. Importantly, miR-133-dependent *cx43* overexpression rescues *esco2*-dependent growth defects. **Conclusions:** These results conceptually link ODDD to cohesinopathies and provide evidence that *ESCO2* may play a transcriptional role critical for human development. *Developmental Dynamics* 245:7–21, 2016. © 2015 Wiley Periodicals, Inc.

Key words: *esco2/ECO1/CTF7*; *cx43/gja1*; gap junctions; Roberts syndrome (RBS); oculodentodigital dysplasia (ODDD); cohesinopathy

Submitted 10 April 2015; First Decision 9 September 2015; Accepted 24 September 2015; Published online 5 October 2015

Introduction

The skeleton supports soft tissues, provides for muscle attachment and protects internal organs from risk of injury. Additional functions include calcium and phosphorus storage, blood cell production and immune response. Given this diverse array of functionality, mutations that affect skeletal functions exhibit pleiotropic defects that include osteoporosis, osteoarthritis, and hematopoietic and immunity deficiencies. Aberrations in skeletal development, especially long bone growth and morphogenesis, are also components of several multi-spectrum developmental abnormalities such as Roberts syndrome (RBS) and Cornelia de Lange syndrome (CdLS). In addition to severe long-bone growth defects and missing digits, both RBS and CdLS patients may exhibit craniofacial abnormalities, cleft palate, syndactyly, organ defects, and severe mental retardation (Liu and Krantz, 2009; Mannini et al., 2010).

Recent genetic mapping studies reveal that mutations in cohesin pathways are responsible for RBS and CdLS disorders, as well as a host of related diseases collectively termed cohesinopathies (Krantz et al., 2004; Tonkin et al., 2004; Schule et al., 2005; Vega et al., 2005; Musio et al., 2006; Deardorff et al., 2007,

2012a,b; Gordillo et al., 2008; Van der Lelij et al., 2010; Yuan et al., 2015). Elucidating the molecular basis of these disorders span topics of both chromosome segregation and transcriptional regulation (Rudra and Skibbens, 2013). For instance, RBS arises from mutations in *ESCO2*. High fidelity chromosome segregation requires that sister chromatids be identified from DNA synthesis (S-phase) to anaphase onset during mitosis (M-phase). Identity is achieved by cohesin complexes that tether together sister chromatids. *ESCO2* is an acetyltransferase that converts chromatin-bound cohesins to a tether-competent state (Skibbens et al., 1999; Toth et al., 1999; Ivanov et al., 2002; Zhang et al., 2008; Unal et al., 2008; Ben-Shahar et al., 2008). Thus, it is not surprising that cells isolated from RBS patients exhibit mitotic failure, elevated levels of apoptosis, reduced proliferation and genotoxic hypersensitivities (Horsfield et al., 2012; Mehta et al., 2013). On the other hand, CdLS arises from mutations in the cohesin genes *SMC1A*, *SMC3*, and *RAD21*, the cohesin deposition factor encoded by *NIPBL*, and the de-acetylase encoded by *HDAC8* that targets *SMC3* (Krantz et al., 2004; Tonkin et al., 2004; Musio et al., 2006; Deardorff et al., 2007, 2012a,b). Intriguingly, CdLS patient cells typically exhibit normal mitosis and retain a euploid genomic state, revealing that CdLS instead arises mainly through transcriptional dysregulation (Liu and Krantz, 2009; Dorsett and

*Correspondence to: M. Kathryn Iovine and Robert V. Skibbens, Department of Biological Science, 111 Research Drive, Lehigh University, Bethlehem, PA 18015. E-mail: rvs3@Lehigh.edu and mki3@Lehigh.edu

Article is online at: <http://onlinelibrary.wiley.com/doi/10.1002/dvdy.24354/abstract>
© 2015 Wiley Periodicals, Inc.

Merkenschlager, 2013). A transcriptional basis of CdLS is supported by findings that cohesins are critical for (1) transcription termination, (2) enhancer-promoter registration, (3) CTCF-insulator recruitment and (4) POLII transitioning from a paused to elongating state (Dorsett and Merkenschlager, 2013). Despite the similarities to CdLS, a transcriptional basis for RBS that involves ESCO2 remains undefined.

The zebrafish caudal fin contains 16 to 17 segmented bony fin rays with new growth occurring by the distal addition of bony segments and associated fin ray joints (Goss and Stagg, 1957; Haas, 1962). Because of its simple structure, rapid regeneration following amputation, and the ability to knockdown gene expression through gene-specific morpholinos, the zebrafish fin is emerging as an excellent model system from which to elucidate tissue and bone growth pathways. For instance, mutations in *connexin43* (*cx43*) cause the *short fin* (*sof^{b123}*) phenotype, which is characterized by defects in bony fin ray growth and joint formation (Iovine et al., 2005; Hoptak-Solga et al., 2008). Missense mutations in human *CX43* cause oculodentodigital dysplasia (ODDD), a genetic disorder that effects both craniofacial and distal skeleton limb development (Paznekas et al., 2003). Thus, the regenerating fin provides clinically relevant insights into highly conserved pathways critical for human skeletal development.

esco2-knockdown studies in zebrafish and medaka embryos produce severe developmental defects, in part recapitulating RBS phenotypes (Monnich et al., 2011; Morita et al., 2012). Interpreting the effects of *esco2*-knockdown in these studies, however, is complicated by large-scale cell death and subsequent indirect or downstream effects. Here, we report on the role of *esco2* during fin regeneration, in the absence of complications produced by whole embryo lethality. The regenerating fin is an ideal system to study the effects of reduced *esco2* on the skeleton in that it avoids the possible confounding effects of reduced *esco2* during development as previously reported. In the current study, results reveal that *esco2* expression is up-regulated in regenerating fins, particularly in the blastema, which is a specialized compartment that contains the majority of proliferative cells. Moreover, *esco2*-knockdown results in defects in both fin regeneration and bony segment length. Importantly, the results reveal that *esco2*-knockdown reduces *cx43* expression and diminishes *cx43* signaling pathways but does not globally reduce other gene expression pathways. In combination, these results suggest the possibility that *Esco2* may act as a specific transcriptional regulator with targets that include *cx43*.

Results

esco2 mRNA is Up-regulated in the Blastema of Regenerating Fins

Despite the fact that *ESCO2* is critical for proper human development (Schule et al., 2005; Vega et al., 2005), little information exists regarding its expression or the molecular basis through which mutations in *ESCO2* result in skeletal disorders. Here, we exploit the adult zebrafish regenerating fin to address both of these fundamental issues in the absence of confounding effects due to embryonic death. To ascertain the temporal regulation of *esco2* expression in regenerating fins, fins were amputated at the 50% level and regenerating tissue harvested at 1, 3, 5, and 8 days postamputation (dpa). The expression of *esco2* was then assessed by whole-mount in situ hybridization (Fig. 1). At 1 dpa, *esco2*

was not detectable. *esco2* was readily apparent at both 3 and 5 dpa with levels starting to diminish at this later time point. By 8 dpa, *esco2* expression was significantly reduced. High *esco2* expression at 3 dpa is consistent with previous studies that map this period as the peak rate of regeneration in the zebrafish fin (Lee et al., 2005; Hoptak-Solga et al., 2008) and suggest that the localization of *esco2* expression might similarly correlate with the highly proliferative blastemal compartment. To test this possibility, 5 dpa fins stained for *esco2* expression by in situ hybridization were cryosectioned. The results reveal that *esco2* expression is specifically up-regulated in the blastemal compartment (Fig. 2). To establish that the probe had access to all *esco2*-positive tissue, 5 dpa fins were cryosectioned before hybridization (Smith et al., 2008). Results from this regimen confirm that *esco2* is expressed specifically within the blastema (Fig. 2). In summary, *esco2* expression is temporally regulated and occurs specifically in the blastemal compartment of the zebrafish regenerating fin.

esco2 is a Critical Regulator of Fin Regeneration and Specifically of Bone Growth

esco2 is an essential gene (Monnich et al., 2011; Whelan et al., 2012; Morita et al., 2012), requiring knockdown strategies to ascertain function in the adult regenerating fin. Therefore, we depleted *Esco2* using morpholino (MO)-mediated knockdown methodologies (Hoptak-Solga et al., 2008; Sims et al., 2009) using one of the two validated MOs for *Esco2* (Monnich et al., 2011). As a control, we used either a custom mismatch morpholino (5MM) containing five mismatches compared with the *esco2* targeting MO or the "standard control" MO from Gene Tools that does not recognize target genes in zebrafish. Uptake is accomplished by first injecting the MO into the blastema of the regenerating fin, followed by electroporation across the fin. All MOs are modified with fluorescein, permitting validation of cellular uptake. Only fins positive for MOs at 1 day postelectroporation (dpe) are kept for further analysis. Procedural details for all knockdown experiments are outlined in Figure 3.

Regenerate length and segment length were evaluated at 4 dpe/7 dpa. All fin regenerate and segment length measurements were obtained from the 3rd fin ray and results compared between injected (*esco2*-MM or *esco2*-MO) and uninjected portions of the same fin, a strategy previously documented as providing for both internal controls and standardized analyses (Iovine and Johnson, 2000; Hoptak-Solga et al., 2008). Uninjected control fins regenerated in a robust manner. *esco2*-MM injected regenerating fins exhibited identical growth to the uninjected control (Fig. 4). In contrast, regenerating fins injected with the *esco2*-MO exhibited a significant decrease in regenerate length compared with uninjected controls within the same fins (Fig. 4), documenting that *esco2* is critical for fin regeneration.

RBS patients exhibit significant bone growth deficiencies, especially in the arms and legs (Horsfield et al., 2012; Mehta et al., 2013). Thus, it became important to quantify the extent that *esco2* depletion may specifically impact bone segment growth in regenerating fins. To address this question, segment length was measured in uninjected, *esco2*-MM injected, and *esco2*-MO injected fins. The results show that segment length in uninjected fish was nearly identical to that of *esco2*-MM injected fish (Fig. 4). However, segment length was significantly reduced in *esco2*-MO injected fish compared with the uninjected side of the same fish fins (Fig. 4). Thus, *esco2* is critical for bone growth

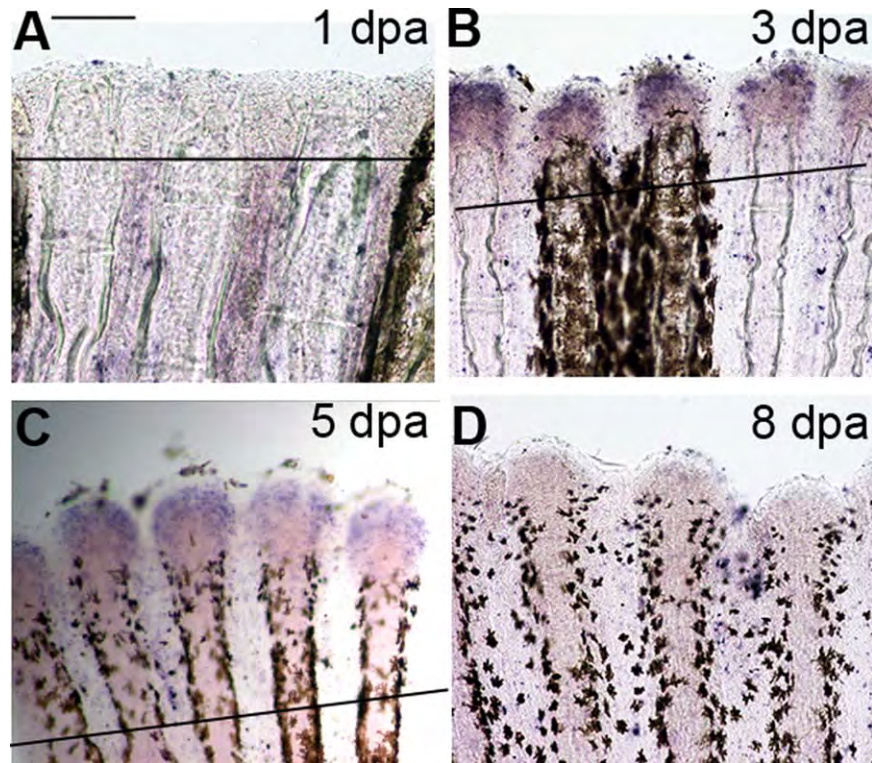


Fig. 1. Time course in situ hybridization of *esco2* in whole-mount regenerating fins. **A:** *esco2* expression in 1 day postamputated (dpa) regenerating fins was largely not detectable. **B,C:** *esco2* expression in 3 dpa regenerating fins was strongly detected at the distal end (B) and began to gradually decline in 5 dpa regenerating fins (C). **D:** Expression of *esco2* was reduced in regenerating fins by 8 dpa. The amputation plane is indicated by a solid line except in 8 dpa regenerating fin (D), where it is out of the field of view. Scale bar = 50 μ m.

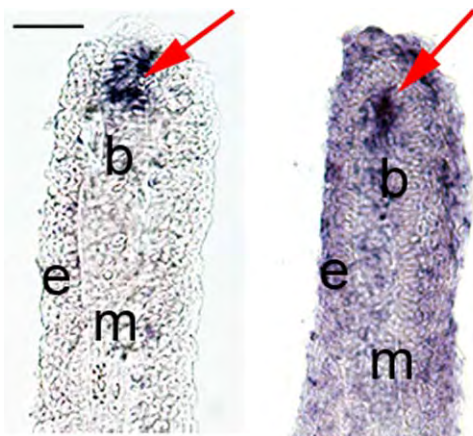


Fig. 2. In situ hybridization of *esco2* in fin cryosections. Left: Cryosection from a whole-mount WT-5 dpa fin treated for in situ hybridization showing tissue specific expression of *esco2* mRNA within the blastema compartment. Right: In situ hybridization was completed on a WT-5 dpa fin cryosection showing a similar pattern of *esco2* expression localized specifically at the blastemal region. Arrows indicate *esco2* expression at blastema. B, blastemal; e, epidermis; m, mesenchyme. Scale bar = 50 μ m.

in regenerating fins, consistent with its role in skeletal development in humans.

To confirm that the *esco2*-MO was effective in reducing Esco2 protein levels, we generated an antibody against Esco2 and verified its specificity using bacterial lysates expressing GST-Esco2. The results show that the anti-Esco2 antibody recognizes GST-Esco2, which migrates at the predicted size of 94 kDa. The anti-

GST antibody also recognizes the GST-Esco2 band at the predicted size of 94 kDa and a 26 kDa band in the GST alone lane (Fig. 5). The anti-Esco2 antibody does not recognize GST alone. To confirm the specificity of the anti-Esco2 antibody, a peptide competition assay was performed. Esco2-directed antibody was preincubated with the peptide that the antibody was generated against. The resulting competed antibody produced a greatly reduced signal, compared with noncompeted antibody, when used to detect GST-Esco2, confirming antibody specificity (Fig. 5). Upon validating the specificity of the Esco2-directed antibody, we tested the effectiveness of the *esco2*-MO to knockdown Esco2 levels in vivo. At 3 dpa, fins were injected with either *esco2*-MM or *esco2*-MO and harvested the next day (1 dpe/4 dpa) to prepare fin lysate (see also Fig. 3). The lysates were used to test for Esco2 reduction by western blot. Quantification of the resulting western blots show that the *esco2*-MO reduces Esco2 protein levels by approximately 70% while robust levels of Esco2 persist in MM injected fins (Fig. 5). The results of the Western blot analyses document the efficacy of the *esco2*-MO to significantly reduce Esco2 protein levels.

Role of *esco2* in Cell Proliferation and Programmed Cell Death

Reduced tissue and bone segment growth in regenerating fins could be due to decreased cell proliferation, increased programmed cell death (PCD), or both. To address possible changes in the level of cell proliferation, we evaluated both 5-bromo-2'-deoxyuridine (BrdU) as a marker for S-phase (Iovine et al., 2005)

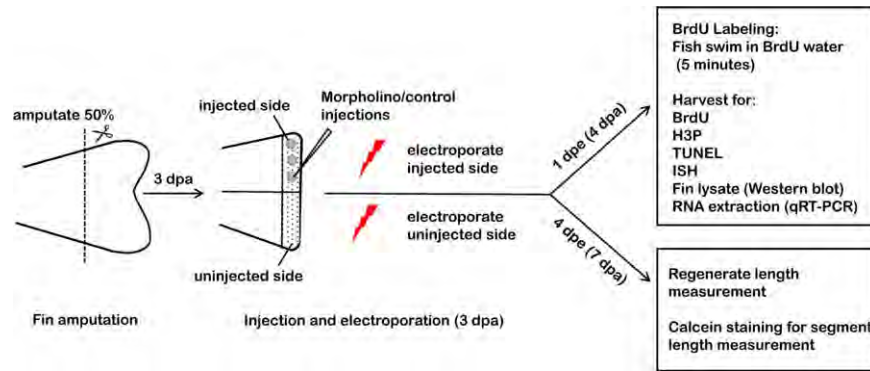


Fig. 3. Timeline of experimental procedure. Fins were amputated at 50% level and allowed to regenerate for 3 days. At 3 dpa, either gene-targeted morpholino or a control morpholino (MO) was injected into half of the regenerating fin, immediately followed by electroporation on both sides. After 24 hr, 1 day postelectroporation (1 dpe/4 dpa), the fins were evaluated by fluorescence microscopy to confirm MO uptake. The fins were harvested at 1 dpe/4 dpa for histone-3-phosphate (H3P) assay, Terminal deoxynucleotidyl transferase dUTP nick end labeling (TUNEL) assay, in situ hybridization (ISH), fin lysate preparation for protein expression by western blot and RNA extraction for qRT-PCR. Note that for protein lysates and for qRT-PCR, all fin rays across the fin were injected with morpholino and electroporated before harvesting at 1 dpe/4 dpa. For 5-bromo-2'-deoxyuridine (BrdU) labeling the MO-injected fins were allowed to swim in 50 μ g/ml of BrdU water for 5 min at 1 dpe/4 dpa and harvested on the same day. For regenerate length and segment length analysis fins were allowed to regenerate longer and were calcein stained at 4 dpe/7 dpa. For each experiment at least 6–8 fish were used per trial and at least 3 independent trials were performed.

and histone-3-phosphate (H3P) as a marker for M phase (Wei et al., 1999). Morpholino-injected fish (where half of the fin was injected with either *esco2*-MO or *esco2*-MM, see also Fig. 3) were allowed to swim in water supplemented with BrdU at 1 dpe/4 dpa and fins harvested immediately. To quantify BrdU staining through which BrdU incorporation could be directly compared between the two fin halves, we compared the ratio of the BrdU-positive domains in the regenerating tip with the total regenerate length. As expected, *esco2*-MM injected and uninjected fins exhibited nearly identical ratios of BrdU labeled cells to regenerate fin length. In contrast, *esco2*-MO injected and uninjected sides produced a significant decrease in the ratio of BrdU labeled cells to regenerate length (Fig. 6), demonstrating fewer dividing progenitor cells at the time of labeling. Next we evaluated H3P-positive cells at 1 dpe/4 dpa (see also Fig. 3). To compare H3P-positive cells between *esco2*-MM and MO injections in fin halves of the same fin, we counted the total number of H3P-positive cells in the 250 μ m area that defines the proliferative blastema, normalizing for the area (Nechiporuk et al., 2002). Regenerating fins in which one fin half was uninjected and the other half injected with *esco2*-MM exhibited nearly identical numbers of H3P-positive cells within this defined area (Fig. 6). In contrast, the *esco2* MO-injected side exhibited a statistically significant reduced level of H3P-staining cells compared with the uninjected sides of the fins (Fig. 6). Thus, cell proliferation appears to play a critical role in skeletal regrowth defects that occur in regenerating fins depleted of Esco2.

To address the possibility that PCD is increased in Esco2 depleted fins, fins were injected with either *esco2*-MM or *esco2*-MO on one half of the fin, the other half uninjected, and the fins were harvested 1 dpe/4 dpa for TUNEL staining (see also Fig. 3). Importantly, we did not detect a noticeable difference in the number of TUNEL-positive cells between the *esco2*-MO injected side and the uninjected side of the same fins (Fig. 7). Statistical analysis confirms that similar numbers of apoptotic cells are present in *esco2*-knockdown and uninjected sides of the same fins (Fig. 7). Thus, it appears that regenerate and bone growth defects that occur upon *esco2*-knockdown can be separated from increased levels of PCD.

esco2 and *cx43* Appear to Function in a Common Pathway

The pattern of *esco2* expression and localization during fin regeneration, coupled with impact of *esco2* depletion on bone segment regrowth, are strikingly similar to those previously reported for *cx43* mutations that cause the *short fin* (*sof*^{b123}) phenotype (Iovine et al., 2005; Hoptak-Solga et al., 2008). Could Esco2 and Cx43 function in a common pathway to influence bone segment growth? To address this possibility, we first tested whether Esco2 function is downstream of Cx43. If true, then *esco2* expression might be reduced in *sof*^{b123} mutant fins. Whole-mount in situ hybridization was performed to monitor *esco2* message levels in wild-type (WT) and *sof*^{b123} regenerating fins. The results show that *esco2* expression levels are nearly identical in regenerating WT and *sof*^{b123} fins (Fig. 8), suggesting that *esco2* is not downstream of *cx43*. An alternate possibility is that *cx43* is downstream of *esco2*. Whole-mount in situ hybridization was performed on *esco2*-knockdown fins (1 dpe/4 dpa, see also Fig. 3) to determine if *cx43* expression is reduced in the half of the fin injected with *esco2*-MO (Fig. 9). Indeed, *cx43* was reduced in fin rays injected with *esco2*-MO and not reduced in either MM control or uninjected controls (Fig. 9). To independently test for *cx43* dependency on *esco2*, we performed quantitative real-time polymerase chain reaction (qRT-PCR) at 1 dpe/4 dpa (see also Fig. 3). The results from three independent *esco2*-knockdown samples show that *cx43* is significantly down-regulated in *esco2*-knockdown regenerating fins (Table 1; Fig. 10). Because reduced cell proliferation is not sufficient to cause reduced *cx43* expression (Govindan and Iovine, 2014; Bhadra and Iovine, 2015), the observed reduction of *cx43* expression is not likely the result of reduced cell proliferation in *esco2*-knockdown fins. In combination, these findings support a model where Cx43 acts downstream of, and may be regulated by, Esco2.

To further examine the possibility that Esco2 and Cx43 function in a common pathway, we next evaluated expression of both *semaphorin3d* (*sema3d*) and *hyaluronan and proteoglycan link protein 1a* (*hapln1a*), two genes recently found to function downstream of *cx43* (Ton and Iovine, 2013; Govindan and

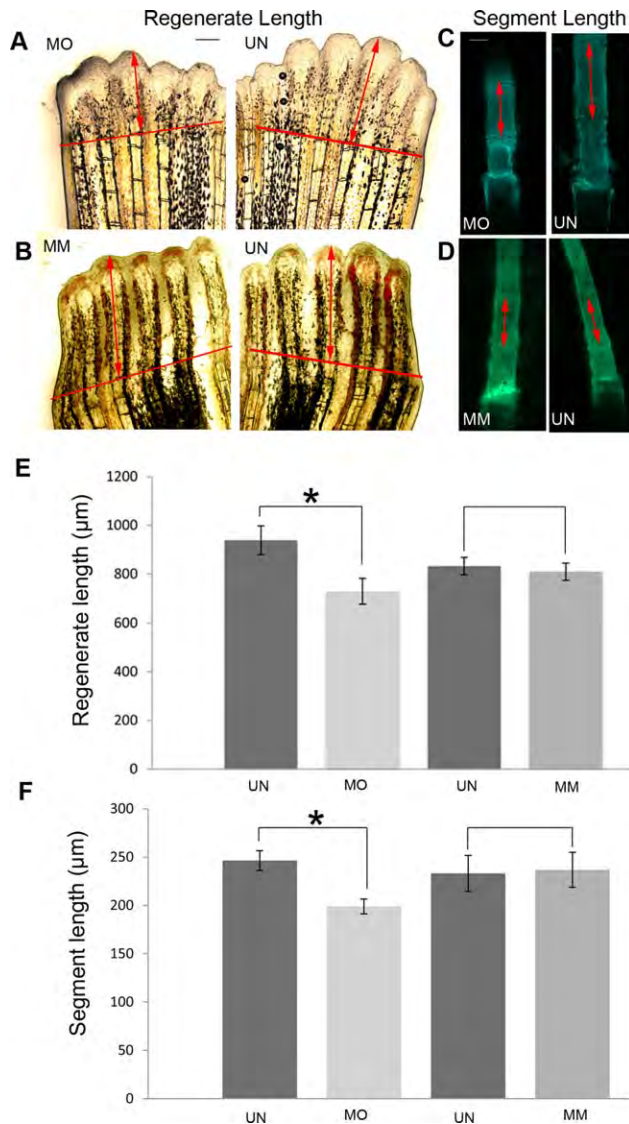


Fig. 4. Morpholino mediated *esco2*-knockdown phenotypes include reduction in regenerate length and bone segment length. **A:** Representative images showing decreased regenerate length in *esco2* morpholino (MO) injected half compared with the uninjected (UN) half of the same fin. **B:** Representative images showing similar levels of regeneration in fins injected with *esco2* mismatch (MM) MO compared with the UN half of the same fin. The red line indicates the amputation plane. Arrows indicate the distance from the amputation plane to the distal end of the 3rd fin ray. **C:** Representative images of calcein stained segments of the 3rd fin ray show shorter bone segments in MO-injected fin half compared with the UN half of the same fin. **D:** Representative images of calcein stained segments of the 3rd fin ray of MM-injected and UN fins reveal bone segments of similar lengths. For all experiments 6–8 fish were used per trial and at least 3 independent trials were performed. The MO/MM was injected/electroporated in 3 dpa fins and was allowed to regenerate for 4 days. For regenerate length and segment length measurements the fins were calcein stained at 4 dpe/7 dpa. For calcein staining, fish were allowed to swim for 10 min in 0.2% calcein (pH7) at room temperature followed by fresh system water for another 10 min. **E:** Graph reveals significant reduction (*) in regenerate length in MO treated fins compared with UN fins. Regenerate length of MM treated fins and UN fins show no significant differences in length. **F:** Graph shows significant reduction (*) in segment length between MO treated fins and UN fins. The segment length of MM treated fins and UN fins show no significant difference. Student's *t*-test was used for determining statistical significance where $P < 0.05$. Standard error is represented by error bars. Scale bar = 50 μm.

Iovine, 2014). If *esco2* is required for *cx43* expression, then *esco2* depletion should also repress these *cx43* targets. We examined the expression levels of *sema3d* and *hapln1a* using qRT-PCR on 3 dpa regenerating fins injected with *esco2*-MO compared with the standard control morpholino. The results show that both *sema3d* and *hapln1a* are significantly down-regulated in MO-injected regenerating fins (Table 1; Fig. 10), consistent with the model that *Esco2* regulates Cx43 signaling pathways that are critical for development. To exclude the possibility that *Esco2* depletion represses all gene expression, we evaluated expression levels of three genes not known to be *cx43*-dependent, *sonic hedgehog* (*shh*), *sprouty 4* (*spry4*), and *mono polar spindle* (*mip1*) (Laforest et al., 1998; Poss et al., 2002; Lee et al., 2005). Expression levels of these genes are not reduced, demonstrating that *Esco2* depletion does not lead to global gene repression. Both *shh* and *spry4* appear to be modestly up-regulated, which could suggest either that *Esco2* antagonizes these genes or that *Esco2*-dependent disruption of cell proliferation indirectly affects gene expression in these pathways. In combination, these results suggest that *Esco2* impacts the transcription of targets that include *cx43*.

If *cx43* truly acts downstream of *Esco2* and *cx43* reduction in part mediates the bone growth defects observed upon *Esco2* knockdown, then we reasoned that Cx43 overexpression might attenuate the regenerate and bone segment growth defects in regenerating fins. To test this prediction, we next attempted to rescue *esco2*-dependent skeletal growth defects by overexpression of Cx43. We used the *Tg(hsp70:miR-133sp^{pd48})* line that harbors an EGFP cDNA followed by three miR-133 binding sites (Ebert et al., 2007; Loya et al., 2009). Prior studies found that miR-133 knockdown by means of this “sponge” transgene increases *cx43* levels during zebrafish heart regeneration (Yin et al., 2012). We confirmed up-regulation of both *cx43* mRNA and Cx43 protein in regenerating fins of this transgenic line treated for heat shock (Fig. 11). Moreover, to rule out the possibility that increased Cx43 leads to an increase in *Esco2*, we further confirmed that the levels of *esco2* mRNA and *Esco2* protein are not up-regulated in this transgenic line treated for heat shock (Fig. 11).

Either transgenic-positive (Tg+) or transgenic-negative (control siblings, Tg-) fins were treated for *esco2*-knockdown (Fig. 12). Four hours postelectroporation, Tg+ and Tg- fish were both heat shocked (HS+) at 37degC for 1 hr. These fish are denoted as Tg+HS+ and Tg-HS+, respectively. Alternatively, a second group of *esco2*-knockdown Tg+ fish was not heat shocked and thus denoted as Tg+HS-. To demonstrate that heat shock alone does not rescue *esco2*-dependent phenotypes, we performed *esco2*-knockdown in Tg-HS+. Results from three independent trials show that *esco2*-knockdown in Tg-HS+ exhibited the predicted growth defects for regenerate fin and bone segment lengths (i.e., the percent similarity between the *esco2*-knockdown side and the uninjected side is low) (Fig. 12). In contrast, *esco2*-knockdown followed by induction of the transgene (causing *cx43* over-expression) in Tg+HS+, exhibited increased regenerate length and segment length, demonstrating Cx43-dependent rescue of the *esco2*-knockdown phenotypes (i.e., the percent similarity between the *esco2*-knockdown side and the uninjected side is significantly increased when *cx43* is overexpressed). We performed the same experiment using *esco2*-MM construct as a negative control. As expected, we did not observe skeletal phenotypes in these fins (data not shown). To demonstrate that

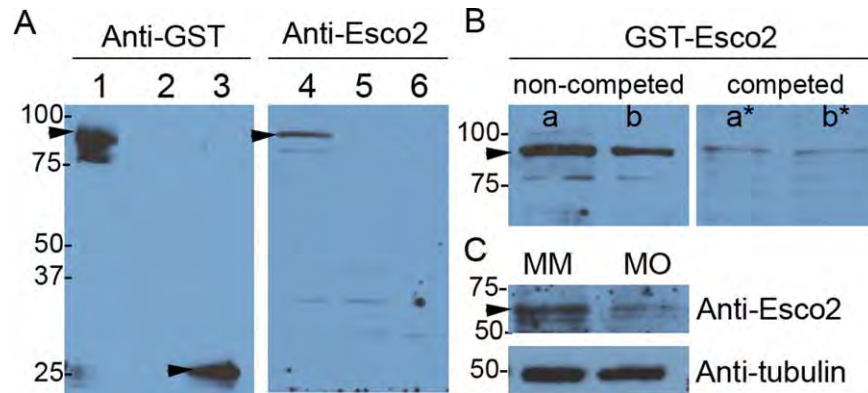


Fig. 5. The Esco2 antibody is specific and MO-mediated *esco2*-knockdown results in decreased levels of Esco2 protein. **A:** Western blot of bacterial lysates expressing either GST-Esco2 or GST. Lanes 1 and 4 are lysates of induced GST-Esco2. Lanes 2 and 5 are lysates of uninduced GST-Esco2. Lanes 3 and 6 are lysates of induced GST. When probed with either the anti-Esco2 antibody or an anti-GST antibody, a major protein band of the predicted size of 94 kDa (indicated by an arrowhead) is detected in the induced GST-Esco2 lysates (lanes 1 and 4), and not in the uninduced GST-Esco2 lysates (lanes 2 and 5). Additional bands below 94 kDa likely represent proteolysis of GST-Esco2. The anti-Esco2 antibody does not detect GST alone, which has a molecular weight of 26 kDa (compare lanes 3 and 6). **B:** Two volumes of bacterial lysates expressing GST-Esco2 were loaded in two identical gels. Preincubation of the anti-Esco2 antibody with the Esco2 peptide (competed lanes a* and b*) significantly reduced the antibody binding compared with noncompeted antibody (lanes a and b). The 94 kDa bands are marked (arrowhead). **C:** Western blot reveals that anti-Esco2 antibody detects a major protein band at 68 kDa from fin lysate prepared from mismatch (MM) control morpholino injected fins and Esco2 knockdown (MO) fins (1 dpe/4 dpa). The blot confirms the reduction of Esco2 protein in the knockdown lysate (MO) compared with the control lysate (MM). The presence of additional bands in the fin lysates may be due to modification or degradation. Tubulin was used as a loading control. The single band marked was used for relative band intensity analysis using the gel analysis tool (ImageJ software). Similar findings were observed in each of three trials.

the rescue of phenotype is heat shock dependent and, therefore, requires overexpression of *cx43*, we performed the same *esco2*-knockdown experiment in the absence of heat shock in Tg + fish (Tg+HS-). Importantly, we did not observe rescue of skeletal phenotypes in fish that carry the transgene but in which we do not induce its expression by means of the heat pulse (Fig. 12). The combination of these experiments provide compelling evidence that Esco2 and Cx43 function in a common pathway, and that the observed *esco2*-dependent skeletal phenotypes are at least partially mediated by reduced *cx43* expression.

Discussion

Cohesinopathies are a growing collection of severe and phenotypically pleiotropic developmental maladies, but at present the molecular mechanisms through which cells and developing organisms respond to cohesion mutations remains unclear (Horsfield et al., 2012; Mehta et al., 2013; Dorsett and Merckenschlager, 2013; Barbero, 2013). For instance, CdLS appears to arise through transcriptional dysregulation that occurs in response to heterozygous or X-linked mutations in *NIPBL*, *SMC1*, *SMC3*, *RAD21*, or *HDAC8*—phenotypes also mimicked in *PDS5* knockout mice (Krantz et al., 2004; Tonkin et al., 2004; Gillis et al., 2004; Musio et al., 2006; Deardorff et al., 2007, 2012a,b; Zhang et al., 2009). In contrast, the sister cohesinopathy RBS, which arises through homozygous mutation of *ESCO2* (Schule et al., 2005; Vega et al., 2005; Gordillo et al., 2008), is thought to arise instead through reduced progenitor cell proliferation and increased mitotic failure and apoptosis (Horsfield et al., 2012; Whelan et al., 2012; Mehta et al., 2013). Our current studies suggest that Esco2 is a critical transcriptional regulator, leading us to speculate that RBS is most likely a transcriptional dysregulation malady. Support for this model is four-fold. First, *esco2*-knockdown reduces transcription of specific cell signaling pathways such as *cx43* (mutations in which disrupt proper development (Paznekas et al., 2003; Iovine

et al., 2005; Musa et al., 2009), but not other developmentally-relevant signaling pathways such as *shh* (Table 1; Fig. 10). Second, recent evidence reveals that Esco2 regulates Notch signaling through binding/sequestration of the intracellular Notch domain (Leem et al., 2011). Notch is required for neuronal differentiation, skeletal development, and hematopoietic lineages, consistent with pleiotropic phenotypes that result in both *esco2* and *notch* mutations (Zanotti and Canalis, 2013). Third, other lines of evidence suggest that ESCO proteins may recruit or link chromatin modifiers to DNA (Choi et al., 2010; Kim et al., 2008). Fourth, our results reveal no significant increase in the incidence of apoptotic cells following *esco2*-knockdown in the blastemal compartment of regenerating fins. At present, we cannot exclude the possibility that a small increase in apoptotic cells is masked by a low but consistent background level required for remodeling in the regenerating fin, but the fact that elevated levels were not discernible in MO-injected fins compared with MM-injected and uninjected matched-fin controls suggests instead that the effects on fin and bone segment regeneration can occur independent of apoptosis. These findings contrast studies involving *esco2*-knockdown in zebrafish and medaka embryos and mice in which reproducible elevations in apoptotic cells were reported (Monnich et al., 2011; Morita et al., 2012; Whelan et al., 2012). However, the effects in those studies are modest. *ESCO2*-knockdown in mice neuroepithelium, for instance, produced severe microcephaly but succeeded in inducing only a two-fold increase in the number of apoptotic cells (Whelan et al., 2012). In zebrafish embryos, *esco2* depletion resulted in Caspase 8 activation that was temporally limited (Monnich et al., 2011). Esco2 depletion also resulted in a four-fold increase in the number of apoptotic cells in zebrafish embryos and global induction of apoptosis in medaka embryos, but such increases that occur in inviable or failing embryos are plausibly downstream events indirectly coupled to *esco2* effects (Monnich et al., 2011; Morita et al., 2012). Thus, it remains possible that apoptosis is not the major clinically relevant etiologic

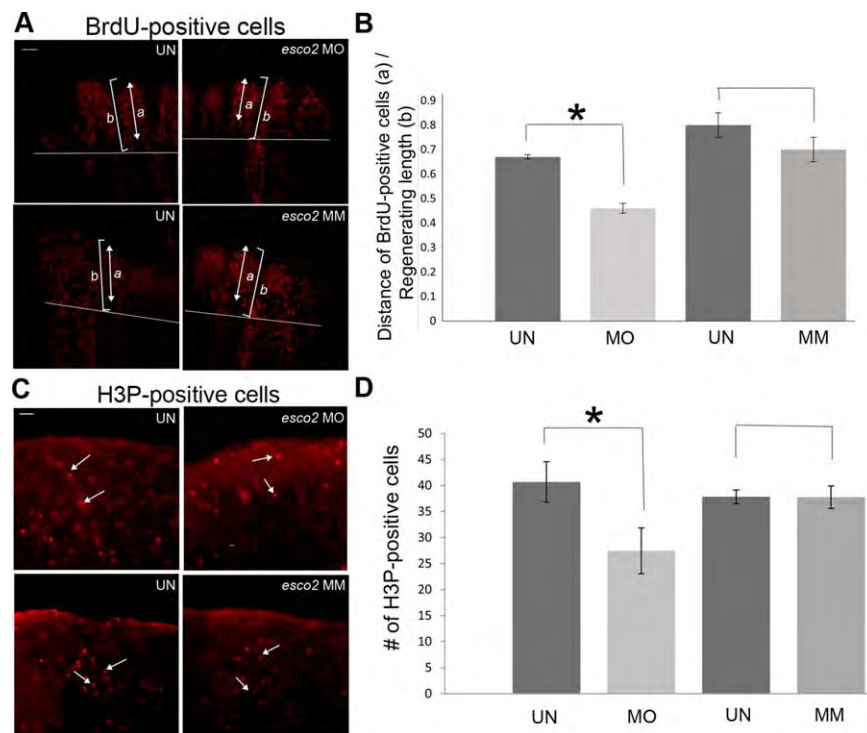


Fig. 6. Role of *esco2* in cell proliferation. **A:** (Top) Representative images of BrdU-positive cells in uninjected (UN) and *esco2*-MO injected (MO) fins. (Bottom) Representative images of BrdU-positive cells in uninjected (UN) and MM injected fins. Briefly, the MO/MM was injected/electroporated in 3 dpa fins and the next day (1 dpe/4 dpa) the fish were allowed to swim in 50 μ g/ml BrdU water for 5 mins and then harvested. For all the experiments at least 6–8 fins were used per trial and at least 3 independent trials were performed. The arrow indicates the span of the BrdU-positive cells from the tip of the 3rd fin ray (a) and the bracket indicates total regenerate length of the 3rd fin ray (b) The amputation plane is shown by a horizontal line. **B:** Graph shows the significant reduction (*) in a/b ratio of BrdU-positive cells in MO injected fins compared with the UN fins. The difference between the MM treated fins and the UN fins is not significantly different. Student's *t*-test was used for determining statistical significance where $P < 0.05$. Standard error is represented by error bars. Scale bar = 100 μ m. **C:** (Top) Representative images of H3P-positive cells in uninjected (UN) and *esco2*-MO injected (MO) fins. (Bottom) Representative images of H3P-positive cells in uninjected (UN) and MM injected fins. The arrows indicate single H3P-positive cells. At least 6–8 fins were used per trial and 3 independent trials were performed. The MO/MM was injected in 3 dpa fins and harvested at 1 dpe/4 dpa. H3P-positive cells were counted by eye from within the distal-most 250 μ m of the 3rd fin ray as previously established. **D:** Graph shows the significant reduction (*) in the average number of H3P-positive cells in MO injected fins compared with the UN fins. The difference between the MM treated fins and the UN fins is not significantly different. Student's *t*-test was used for statistical analysis where $P < 0.05$. Standard error is represented by error bars. Scale bar = 50 μ m.

effect of *esco2* mutation in RBS patients, especially because apoptosis is not a feature of CdLS cells (Tonkin et al., 2004; Castrovano et al., 2009; Revenkova et al., 2009). We hypothesize that the transcriptional dysregulation that arises from *ESCO2* mutations may be the underlying etiologic basis for the developmental abnormalities of RBS—upon which are overlaid cohesion defects, mitotic failure and apoptosis.

Currently, mutation of *ESCO2* represents the sole etiologic agent of the severe developmental disorder Roberts syndrome (RBS) in humans (Vega et al., 2005). We posit that a second revelation from our current study is that *Esco2* may be an upstream regulator of *Cx43* function in zebrafish regenerating fins. For instance, *esco2* depletion not only reduces *cx43* expression, but also expression of *sema3d* and *hapln1a*, two genes in the bone growth signaling pathways that rely upon *Cx43*. Conversely, genes that appear independent of *Cx43*, such as *shh*, *spry4*, and *mps1* were not reduced in *esco2*-knockdown regenerating fins. Notably, the spatial and temporal expressions of *esco2* and *cx43* are nearly identical within the regenerating fin (Iovine et al., 2005; current study). Moreover, the demonstration that overexpression of *cx43* rescues *esco2*-dependent skeletal phenotypes strongly suggests that *Esco2* and *Cx43* function in a common pathway. Inhibition of miR-133 could influence the expression

of genes in addition to *cx43*; thus, we cannot formally rule out the possibility that rescue of *esco2*-phenotypes occurs through a more complex pathway. If our model is correct that *Esco2*-dependent expression of *Cx43* is an important factor in human development, then *cx43* mutation should similarly manifest developmental abnormalities. In fact, mutations of human *CX43* cause ODDD, a malady that includes craniofacial dysmorphias, distal limb skeletal growth defects, and abnormal eye and teeth development (Paznekas et al., 2003; Musa et al., 2009). We note prior studies in which mutation/depletion of either *esco2*, *nipbl*, or *rad21* were found to impact a plethora of developmentally relevant genes, including *CX43/GJA1*, observations that helped to inform the current study (Kawauchi et al., 2009; Monnich et al., 2011). Our findings suggest that *Esco2* function may be coupled to a *Cx43*-dependent signaling pathway previously shown to directly promote proper development. Based on these results, we suggest that ODDD could be a mild form of cohesinopathies.

Conservatively, the current study is consistent with a model that *Esco2* regulates the expression, either directly or indirectly, of *cx43* and its downstream targets (i.e., *sema3d* and *hapln1a*), thereby influencing growth and skeletal patterning (Fig. 13). Future experiments to test this model include measuring *cx43*

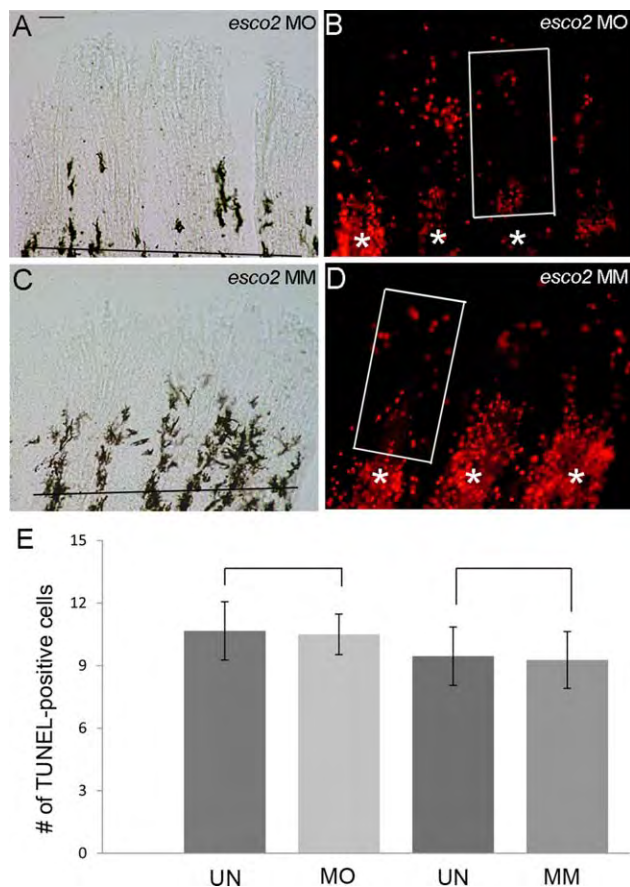


Fig. 7. Role of *esco2* in programmed cell death. **A,B:** Representative bright-field image (A) and TUNEL-positive cells (B) in *esco2*-MO injected fins. **C,D:** Representative bright-field image (C) and TUNEL-positive cells (D) in MM injected fins. At least 6–8 fins were used per trial and 3 independent trials were performed. The MO/MM were injected in 3 dpa fins and harvested at 1 dpe/4 dpa (uninjected control halves not shown). TUNEL-positive cells were counted by eye from within the distal-most 250 μm of the 3rd fin ray. The amputation plane is shown by a horizontal line and * indicates the individual fin rays. High levels of TUNEL-positive cells located at the amputation plane serve as an internal control for staining. The box represents the area used to count the cells. (E) Graph shows similar average numbers of TUNEL-positive cells in either MO injected fins or the MM injected fins, compared with the UN fins. Student's *t*-test was used for determining statistical significance where $P < 0.05$. Standard error is represented by error bars. Bracketed comparisons were not significant. Scale bar = 50 μm .

expression level in RBS patient cells and directly assessing *esco2* localization/regulation of the *cr43* promoter. Alternatively, the impact of Esco2 on the skeleton may occur through its roles in DNA damage repair, DNA replication fork progression, chromosome compaction or ribosome maturation/assembly (Skibbens et al., 1999, 2010, 2013; Unal et al., 2004; Strom et al., 2004; Gard et al., 2009; Terret et al., 2009; Bose et al., 2012; Gerton, 2012). We also note differences in H3P labeling between *esco2*-knockdown in embryos and fins (Monnich et al., 2011, and the current study). As stated previously, whole embryos respond to *esco2*-knockdown through tissue, organ and whole embryo failure, which likely produce multiple downstream consequences superimposed on direct effects. It is possible, however, that the outcome of *esco2* knockdown may be different during development compared with regeneration. For example, *esco2* knockdown in embryos (i.e., during deployment of developmental programs)

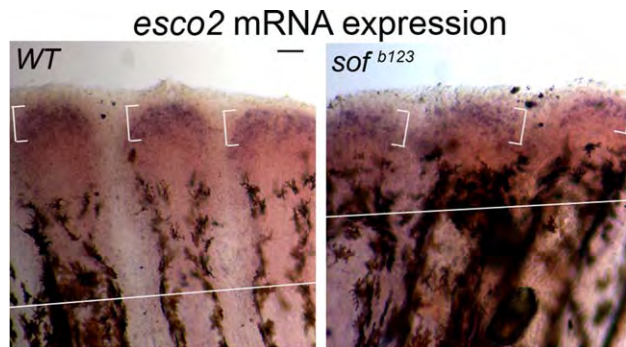


Fig. 8. Expression of *esco2* mRNA in WT and *short fin (sof^{b123})* fins by whole-mount in situ hybridization. WT and *sof^{b123}* fins were amputated at 50% level and allowed to regenerate for 5 days. At 5 dpa, the fins were harvested. At least six to eight fins were used per trial and 3 independent trials were performed. Left: Whole-mount in situ hybridization (ISH) on WT-5 dpa regenerating fins showing *esco2* expression. Right: Whole-mount ISH on *sof^{b123}* -5 dpa regenerating fins shows similar expression levels of *esco2*. The brackets represent the zone of *esco2* expression. Scale bar = 50 μm .

may cause increased aneuploidy (and, therefore, more cell death and mitotic arrest) and transcriptional deregulation (developmental defects), while during regeneration *esco2* knockdown preferentially influences gene expression that leads predominantly to reduced cell proliferation and developmental defects.

Experimental Procedures

Statement on the Ethical Treatment of Animals

This study was carried out in strict accordance with the recommendations in the Guide for the Care and Use of Laboratory Animals of the National Institutes of Health. The protocols used for this manuscript were approved by Lehigh's Institutional Animal Care and Use Committee (IACUC) (Protocol identification # 128, approved 11/16/2014). Lehigh University's Animal Welfare Assurance Number is A-3877-01. All experiments were performed to minimize pain and discomfort.

Housing and Husbandry

Zebrafish (*Danio rerio*) were housed in a re-circulating system built by Aquatic Habitats (now Pentair). Both 3-L tanks (up to 12 fish/tank) and 10-L tanks (up to 30 fish/tank) were used. The fish room had a 14:10 light:dark cycle. Room temperature was tightly regulated and varied from 27 to 29degC (Westerfield, 1993). Water quality was monitored automatically and dosed to maintain conductivity (400–600 μS) and pH (6.95–7.30). Nitrogen levels were maintained by a biofilter. A 10% water change occurred daily. Recirculating water was filtered sequentially through pad filters, bag filters, and a carbon canister before circulating over ultraviolet lights for sterilization. Fish were fed three times daily, once with brine shrimp (hatched from INVE artemia cysts) and twice with flake food (Aquatox AX5) supplemented with 7.5% micropellets (Hikari), 7.5% Golden Pearl (300–500 micron, Brine Shrimp direct), and 5% Cyclo-Peeze (Argent).

Zebrafish Strains and Surgical Procedures

The zebrafish strains used in this study were wild-type (C32), *sof^{b123}* (Iovine and Johnson, 2000), and *Tg(hsp70:miR-133sp^{pd48})*

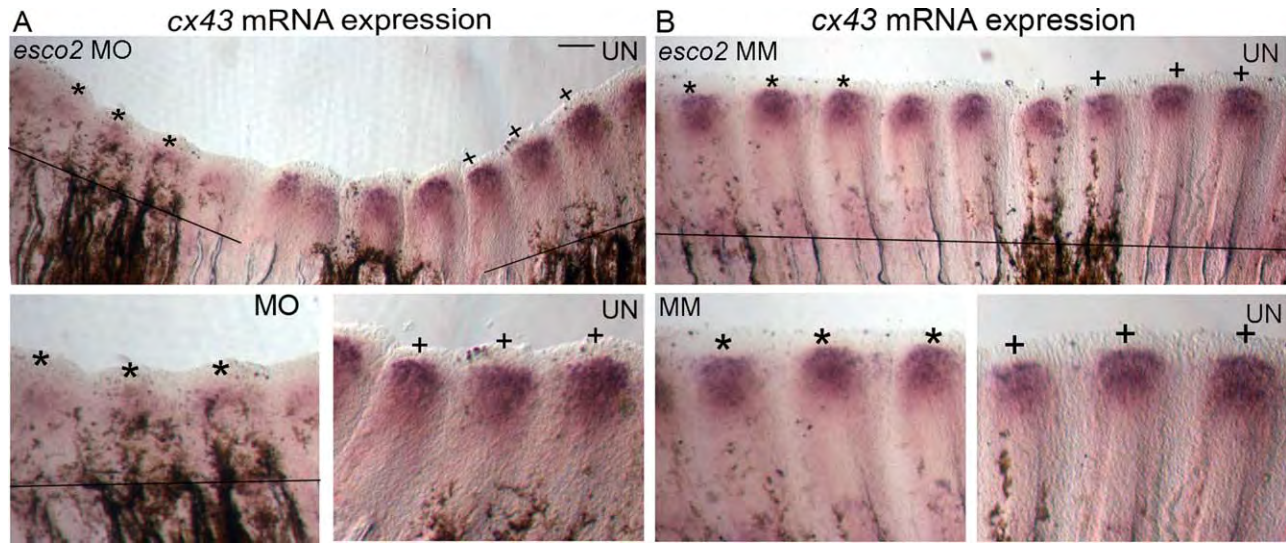


Fig. 9. In situ hybridization on morpholino mediated *esco2*-knockdown fins shows reduced levels of *cx43* expression. The MO/MM was injected in 3 dpa fins and fins were harvested at 1 dpe/4 dpa. The amputation plane is identified by black lines unless it is out of the field of view (i.e., as occurs in most of the higher magnification images). The fin in panel A appears curved because there was less growth on the *esco2*-knockdown side compared with the uninjected side. **A:** (Top) Representative image of a fin with *esco2*-knockdown side (*esco2* MO) showing decreased staining of *cx43*, compared with the uninjected side (UN). (Bottom left) Higher magnification of the knockdown side (MO) of the same fin (fin rays from top image marked by *) showing reduced *cx43* expression. (Bottom right) Higher magnification of the uninjected side (UN) of the same fin (fin rays from top image marked by +) showing robust *cx43* expression. **B:** (Top) Representative image of a fin microinjected with *esco2*-MM in one half and the other side uninjected (UN) reveal similar levels of *cx43*. (Bottom left) Higher magnification of the *esco2*-MM injected side (MM) of the same fin (fin rays from top image marked by *) showing *cx43* expression. (Bottom right) Higher magnification of the uninjected side (UN) of the same fin (fin rays from top image marked by +) showing similar *cx43* expression levels. Scale bar = 100 μ m.

TABLE 1. Quantitative RT-PCR Confirms Changes in Gene Expression

| Gene | Average $C_{T(\text{esco2 KD})}$ | Average C_T (keratin) | ΔC_T <i>esco2</i> KD-keratin ^a | ΔC_T <i>esco2</i> MM-keratin ^a | $\Delta\Delta C_T$ $\Delta C_{T(\text{MO})} - \Delta C_{T(\text{MM})}$ ^b | Fold difference relative to MM ^c |
|----------------|----------------------------------|-------------------------|---------------------------------------------------|---------------------------------------------------|-------------------------------------------------------------------------------------|---------------------------------------------|
| <i>cx43</i> | 23.31 \pm 0.11 | 17.14 \pm 0.15 | 6.16 \pm 0.19 | 5.21 \pm 0.14 | 0.95 \pm 0.24 | 0.51 (0.43–0.61) |
| <i>sema3d</i> | 24.25 \pm 0.15 | 17.25 \pm 0.07 | 7.0 \pm 0.16 | 6.05 \pm 0.12 | 0.94 \pm 0.21 | 0.52 (0.44–0.6) |
| <i>hapln1a</i> | 24.43 \pm 0.05 | 18.09 \pm 0.04 | 6.34 \pm 0.07 | 5.57 \pm 0.42 | 0.85 \pm 0.42 | 0.58 (0.43–0.78) |
| <i>mps1</i> | 22.27 \pm 0.08 | 17.72 \pm 0.08 | 4.55 \pm 0.12 | 4.47 \pm 0.34 | -0.08 \pm 0.36 | 0.94 (0.73–1.21) |
| <i>shh</i> | 22.7 \pm 0.1 | 19.51 \pm 0.05 | 3.24 \pm 0.11 | 3.53 \pm 0.14 | -0.28 \pm 0.18 | 1.21 (1.07–1.38) |
| <i>spry4</i> | 23.3 \pm 0.08 | 19.35 \pm 0.1 | 3.91 \pm 0.13 | 4.45 \pm 0.31 | -0.54 \pm 0.34 | 1.45 (1.14–1.85) |

^aThe ΔC_T value is determined by subtracting the average Keratin C_T value from the average Gene C_T value. The standard deviation of the difference is calculated from the standard deviations of the gene and Keratin values using the Comparative Method.

^bThe calculation of $\Delta\Delta C_T$ involves subtraction by the ΔC_T calibrator value. This is subtraction of an arbitrary constant, so the standard deviation of $\Delta\Delta C_T$ is the same as the standard deviation of the ΔC_T value.

^cThe range given for gene relative to MM is determined by evaluating the expression: $\hat{\Delta} - \Delta\Delta C_T$ with $\Delta\Delta C_T + s$ and $\Delta\Delta C_T - s$, where s = the standard deviation of the $\Delta\Delta C_T$ value.

(Yin et al., 2012). Caudal fin amputations, fin regeneration, and harvesting were done as previously described (Sims et al., 2009; Ton and Iovine, 2013; Govindan and Iovine, 2014). Briefly, fish were first anaesthetized in 0.1% tricaine solution and their caudal fin rays amputated to the 50% level using a sterile razor blade and visualized using a dissecting scope. Fin regeneration proceeded until the desired time period depending on the type of experiment. At the required time point, the regenerated fins were harvested and fixed in 4% paraformaldehyde (PFA) in phosphate buffered saline

(PBS) overnight at 4degC. The fins were then dehydrated in 100% methanol and stored at 20degC until further use.

Gene Knockdown by Morpholino Injection and Electroporation

All morpholinos (MOs) used in the study were fluorescein-tagged and purchased from Gene Tools, LLC. The MOs were reconstituted in sterile water to a final concentration of 1 mM. The sequences

for MOs used in the study are as follows: MO targeted against *esco2* (*esco2*-MO: 5'-CTCTTTCGGGATAACATCTTCAATC-3', from Monnich et al., 2011), *esco2* -5-base mismatch control MO

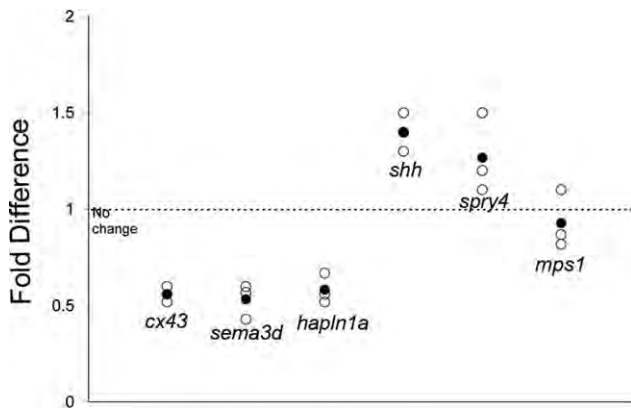


Fig. 10. *cx43* and *cx43*-dependent target genes are reduced following *esco2*-knockdown. The fold difference values from qRT-PCR are shown. A fold difference of 1 indicates no change with respect to standard MO treated fins. Three independent *esco2*-knockdown (KD) samples were prepared. Each sample was tested in duplicate (trials 1–3) for *cx43*, *sema3d*, *hapln1a*, *shh*, *spry4*, and *mps1*, and compared with the internal reference gene. The individual trials are represented by circles and the averages are represented by solid circles.

(*esco2*-MM: 5'-CTCTTTCGGGATAACATCTTCAATC-3', and Gene Tools standard control MO (5'-CCTCTTACCTCAGTTACAATTATA-3'). Microinjection and electroporation procedures were carried out as described previously (Thummel et al., 2006; Hoptak-Solga et al., 2008; Sims et al., 2009). Briefly, caudal fins were amputated at 50% level. At 3 days postamputation (3 dpa), fish were anesthetized and MOs injected using a Narishige IM 300 Microinjector. Approximately 50 nl of MO was injected per ray into either the dorsal or ventral side of the regenerating fin tissue (approximately first five to six bony fin rays), keeping the other side uninjected. The uninjected side served as the internal control. Immediately after injection, both sides of the fin were electroporated using a CUY21 Square Wave electroporator (Protech International Inc). To minimize nonspecific effects of the electroporation procedure, both sides of the fin were electroporated. The following parameters were used during electroporation: ten 50-ms pulses of 15 V with a 1-s pause between pulses. These fish were returned back to the system water for regeneration to proceed. After 24 hr (i.e., 1 day postelectroporation (1 dpe), which is equivalent to 4 dpa, the injected side of the fins were evaluated by fluorescence using a Nikon Eclipse 80i Microscope (Diagnostic Instruments) to confirm MO uptake. The MO injected fins were evaluated for regenerate length, segment length, cell proliferation, cell death, in situ hybridization, protein levels by Western blots and RNA levels by qRT-PCR. For fins used for

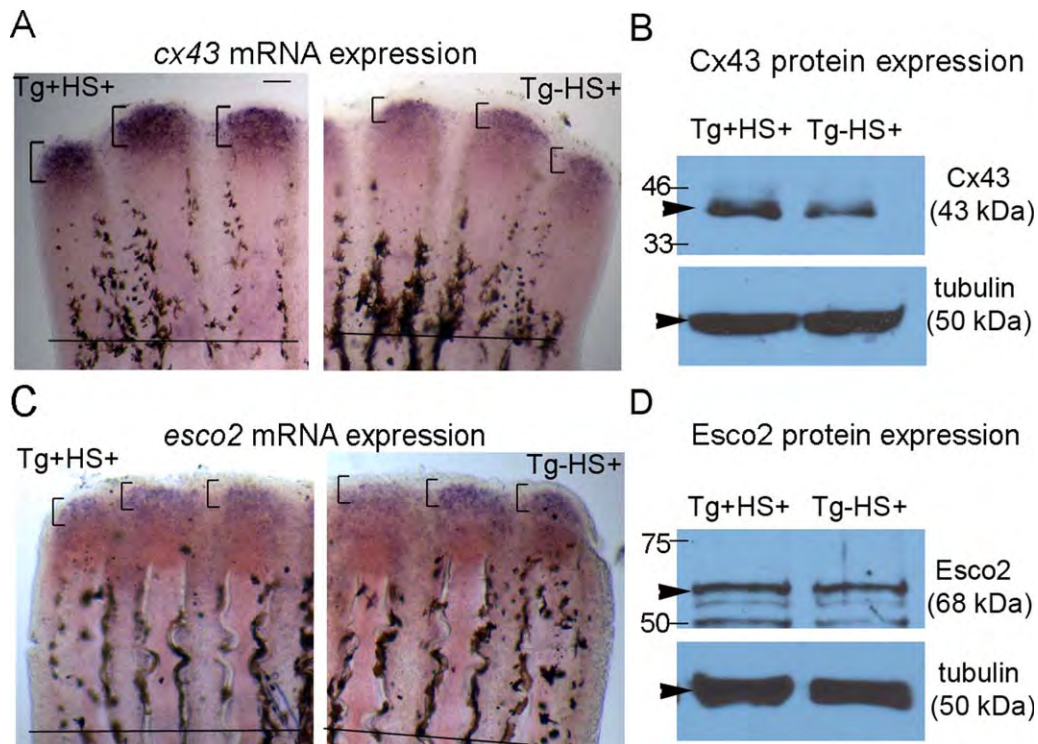


Fig. 11. Up-regulation of both *cx43* mRNA and Cx43 protein in regenerating fins of the transgenic line treated for heat shock. **A:** Expression of *cx43* mRNA in transgenic *hsp70:miR-133sp^{pd48}*-positive with heat shock (Tg+HS+) and *hsp70:miR-133sp^{pd48}*-negative with heat shock (Tg-HS+) fins by whole-mount ISH. The Tg+HS+ fins show a higher expression of *cx43* mRNA compared with Tg-HS+ fins. The brackets mark the zone of *cx43* expression in each fin ray and the horizontal line represents the amputation plane. Scale bar = 50 μ m. **B:** Western blot reveals a 50% increase of Cx43 protein levels (normalized to tubulin) in fin lysates of Tg+HS+ compared with Tg-HS+. Tubulin was used as a loading control. The bands marked were used for relative band intensity analysis using the gel analysis tool (ImageJ software). **C:** Expression of *esco2* mRNA in transgenic *hsp70:miR-133sp^{pd48}*-positive with heat shock (Tg+HS+) and *hsp70:miR-133sp^{pd48}*-negative with heat shock (Tg-HS+) fins by whole-mount ISH. Tg+HS+ and Tg-HS+ fins show similar expression level of *esco2* mRNA. The brackets mark the zone of *esco2* expression in each fin ray and the horizontal line represents the amputation plane. Scale bar = 50 μ m. **D:** Western blot reveals the Esco2 protein expression (normalized to tubulin) is nearly similar (90%) in fin lysates of Tg+HS+ and Tg-HS+. Tubulin was used as a loading control. The single band marked was used for relative band intensity analysis using the gel analysis tool (ImageJ software).

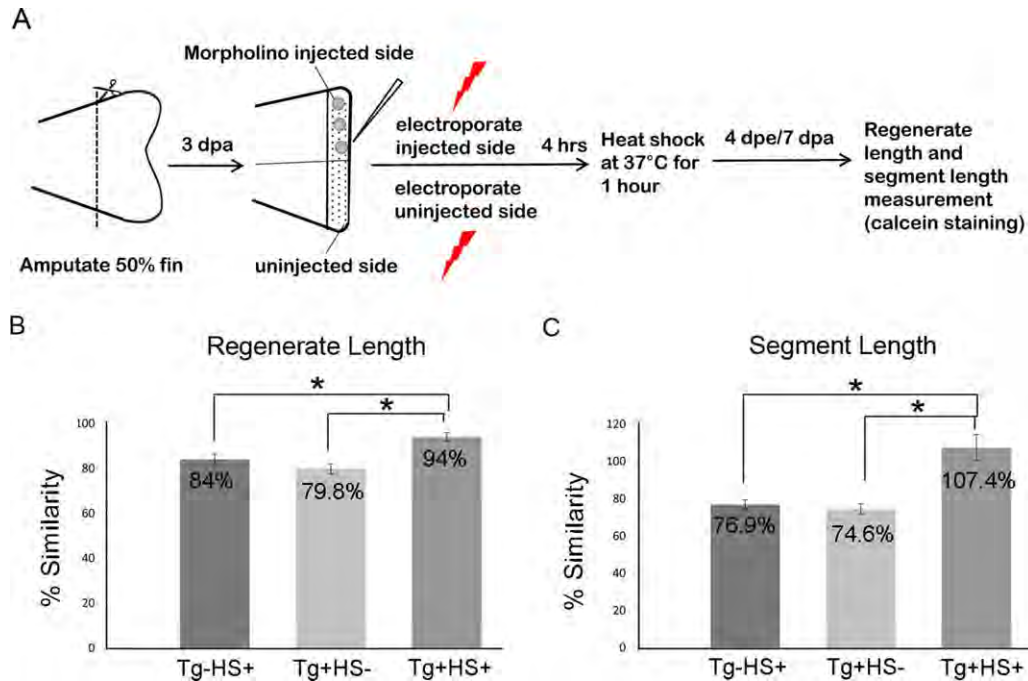


Fig. 12. Overexpression of *cx43* rescues *esco2* knockdown phenotypes. **A:** Figure depicting the timeline of fin amputation, morpholino injection and electroporation, heat shock, and data analysis. The 3 groups included in this experiment were Tg+HS- (transgenic *hsp70:miR-133sp^{pd48}*-positive, heat shock), Tg+HS+ (transgenic *hsp70:miR-133sp^{pd48}*-negative, heat shock) and Tg+HS- (transgenic *hsp70:miR-133sp^{pd48}*-positive, not heat shocked). Briefly, fins from all three groups were amputated at 50% level and allowed to regenerate for 3 days. At 3 dpa, morpholino was injected to one half of the regenerating fin tissue, immediately followed by electroporation on both sides. After an interval of 4 hr fish receiving heat shock were shifted to 37degC for 1 hr. Induction of the transgene expression upon heat shock was confirmed after 24 hr by screening for GFP-positive fins in the Tg+HS+ group. The control groups (Tg-HS+ and Tg+HS-) were negative for GFP expression. For ISH experiments, the fins were harvested at 1 dpe/4 dpa. For measurement of regenerate length and segment length, fins were calcein stained at 4 dpe/7 dpa. For each experiment, at least 6–8 fish were used per trial and at least 3 independent trials were performed. **B:** Graph reveals significant (*) rescue of *esco2*-dependent segment length defects in heat shocked *miR-133sp^{pd48}*-positive *esco2*-knockdown fins (Tg+HS+) compared both with heat shock transgene-negative (Tg-HS+) and with *miR-133sp^{pd48}*-positive with no heat shock (Tg+HS-). Measurements from the injected side and the uninjected side of the same fin were used to calculate percent similarity and the average was calculated for each group. Note that a percent similarity of 100% indicates no difference between the knockdown side and the control sides of the fin. Student's *t*-test was used for determining statistical significance where $P < 0.05$. Standard error is represented by error bars. **(C)** Graph reveals significant (*) rescue of *esco2*-dependent regenerate length defects in heat shocked *miR-133sp^{pd48}*-positive *esco2*-knockdown fins (Tg+HS+) compared both with heat shocked transgene-negative (Tg-HS+) and with *miR-133sp^{pd48}*-positive in the absence of heat shock (Tg+HS-). Measurements from the injected side and the uninjected side of the same fin were used to calculate percent similarity and the average was calculated for each group. Note that a percent similarity of 100% indicates no difference between the knockdown side and the control sides of the fin. Student's *t*-test was used for determining statistical significance where $P < 0.05$. Standard error is represented by error bars.

lysate preparation or for qRT-PCR, all fins were injected and electroporated before harvesting.

Regenerate Length and Segment Length Measurement and Analysis

At 4 dpe/7 dpa, MO injected (*esco2*-MO or *esco2*-MM) fins were calcein stained before measuring regenerate length and segment length (Du et al., 2001; Sims et al., 2009). Briefly, fish were allowed to swim for 10 min in 0.2% calcein (pH 7) at room temperature followed by swimming in fresh system water for another 10 min. The fish were anaesthetized and imaged using Nikon Eclipse 80i Microscope equipped with a SPOT-RTKE digital camera (Diagnostic Instruments) and SPOT software (Diagnostic Instruments). All measurements were performed on the longest fin ray (3rd fin ray) from the ventral or dorsal most lobe of the caudal fin, as previously established (Iovine and Johnson, 2000). Images used to measure regenerate length and bone segment length were analyzed using Image Pro software. For fin regenerate length, measurements were based on amputation site to the

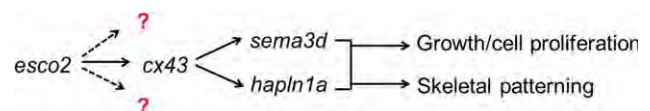


Fig. 13. New model depicts the connection between Esco2 and Cx43 skeletal patterning pathway during fin regeneration. Proposed pathway for Esco2 regulation of *cx43* expression levels and genes downstream of *cx43*. Esco2 may have additional targets.

distal tip of the 3rd fin ray. For bone segment length, the distance between the first two joints formed following regeneration was measured. For each experiment, at least six to eight fish were used per trial and at least three independent trials were performed. Student's *t*-test ($P < 0.05$) was used for statistical analysis.

RNA Probe Preparation and In Situ Hybridization on Whole-Mount and Cryosectioned Fins

RNA probes were made using linear PCR product as template, where the T7 RNA polymerase binding site was included in the

reverse primer. The *cx43* template was made as described (Iovine et al., 2005). The *esco2* product was generated using gene-specific primers (forward primer- 5'AGCAGGGACCTTCTACAGCA3' and reverse primer 5'TAATACGACTCACTATAGGGGGGATCATCTGGAAGAACG3'). RNA probes were labeled with digoxigenin (DIG) following manufacturer instructions (Roche). In situ hybridization (ISH) was performed on WT fins of different time points (1, 3, 5, and 8 dpa) and 5 dpa *sof^{b123}* fins. Briefly, fins were amputated at 50% level and harvested at the appropriate time point. For ISH on knockdown fins, MO (*esco2*-MO or *esco2*-MM) was injected and electroporated on WT-3 dpa fins and harvested after 24 hr (1 dpe/4 dpa). For ISH on whole-mount fins, the standard protocol was followed (Ton and Iovine, 2013; Govindan and Iovine, 2014). For ISH on transgenic *hsp70:miR-133sp^{pd48}*-positive and -negative fins, 3 dpa fish were heat shocked at 37degC for 1 hr and harvested after 24 hr (1 dpe/4 dpa). For all ISH experiments, approximately six to eight fins were used per trial and three independent trials were performed. A Nikon Eclipse 80i Microscope equipped with a SPOT-RTKE digital camera (Diagnostic Instruments) and SPOT software (Diagnostic Instruments) was used to acquire images.

ISH on sections was done as described with the following modifications (Smith et al., 2008). WT-5 dpa fins were first rehydrated sequentially by methanol-PBS washes, cryosectioned, and stored at -20degC. Slides were defrosted for approximately 1 hr before hybridization and section locations marked with a hydrophobic barrier pen (ImmEdge Pen; PAP pen, VWR Laboratories). RNA probe was mixed with hybridization buffer: 1 × salt solution (NaCl, Tris HCl, Tris Base, Na₂HPO₄, and 0.5 M EDTA), 50% deionized formamide (Sigma), 10% dextran sulfate, 1 mg/ml tRNA, and 1 × Denhart's (Fisher) and denatured by incubating at 70degC for 5 min. The denatured probe mix was added to the sections and hybridized overnight at 65degC. Slides were washed at 65degC with a 1 × SSC, 50% formamide and 0.1% Tween-20 solution, rinsed with MABT (100 mM Maleic acid, 150 mM NaCl, and 0.1% Tween-20) and incubated in a blocking solution (MABT, goat serum, and 10% milk) for 2 hr. Anti-DIG antibody (1:5,000) was diluted in MABT and the slides were incubated overnight at 4degC. Slides were washed 4 × in MABT, 2 × in alkaline phosphatase staining buffer (100 mM Tris, pH 9.5, 50 mM MgCl₂, 100 mM NaCl, and 0.1% Tween20), then incubated overnight at 37degC in 10% polyvinyl alcohol staining solution and NBT/BCIP (nitroblue tetrazolium/5-bromo-4-chloro-3-indolyl phosphate) stock solution (Roche). The reaction was stopped by washing extensively with PBST. Sections were mounted in 100% glycerol and images acquired using a Nikon Eclipse 80i Microscope equipped with a SPOT-RTKE digital camera (Diagnostic Instruments) and SPOT software (Diagnostic Instruments).

Immunoblotting and Esco2 Antibody

Escherichia coli lysates from cells expressing either GST or GST-Esco2 fusion protein (protein expression was induced using 0.3 mM IPTG for 4 hr) were prepared as described (Gerhart et al., 2012). Briefly, cells from 1 ml of culture were pelleted and lysed using 50 µg/ml lysozyme in lysis buffer (100 mM Tris-HCl pH 7.5, 50 mM NaCl, 10 mM EDTA pH 8, complete protease inhibitor cocktail, Roche). To this mixture, 2.2 N NaOH and 8% BME were added. Protein precipitation was carried out using 55% TCA followed by wash with 0.5% TCA. The protein pellets were resuspended in 2 × sodium dodecyl sulfate buffer. GST or GST-Esco2

were detected by Western blot using anti-GST antibody (Santa Cruz, 1:5,000) or affinity-purified anti-Esco2 (1:1,000). Affinity purified polyclonal Anti-Esco2 was generated in rabbit against the N-terminal peptide LSRKRKHGSPDAESC (Genscript) and used at a concentration of 1:1,000 for the noncompeted Western blot. For the anti-Esco2 antibody specificity assay, identical gels were loaded with decreasing volumes of the GST-Esco2 protein samples. For the competed blot, the anti-Esco2 antibody was preincubated with the Esco2 peptide (100 µM). The blots were incubated with primary antibody overnight at 4degC.

Fin lysates were prepared as previously described (Hoptak-Solga et al., 2008; Gerhart et al., 2012; Govindan and Iovine, 2014). Briefly, approximately 9–10 MO-injected (*esco2* MO or *esco2* MM) 1 dpe/4 dpa regenerating fins were pooled, and then suspended in incubation buffer (136.8 mM NaCl, 5.36 mM KCl, 0.34 mM Na₂HPO₄, 0.35 mM KH₂PO₄, 0.8 mM MgSO₄, 2.7 mM CaCl₂, 20 mM HEPES with pH adjusted to 7.5) supplemented with protease inhibitor (Thermo scientific, Halt™ Protease and Phosphatase Inhibitor Cocktail, 100X). The harvested fin tissue was homogenized by a tissue homogenizer (Bio-Gen, PRO 200) at high speed (3 ×) for 5 sec with 10-sec cooling intervals. Homogenized samples were centrifuged at 200 g for 10 min at 4degC and supernatant protein levels normalized according to Bradford assays. Note that for preparation of proteins lysate from heat shocked *Tg(hsp70:miR-133sp^{pd48})*-positive and *Tg(hsp70:miR-133sp^{pd48})*-negative fish, 37degC heat shock was performed for 1 hr at 3 dpa and fins harvested at 1 dpe/4 dpa as previously described.

GST, Esco2, Cx43, or tubulin was detected using anti-GST (1:5,000) (Santa Cruz), anti-Esco2 (1:1,000), anti-Cx43 (1:1,000, Hoptak-Solga et al., 2008) or anti-α-tubulin (1:1,000) (Sigma), followed by exposure to peroxidase-conjugated goat anti-rabbit IgG (GST, Esco2 and Cx43) or goat anti-mouse IgG (tubulin) (Pierce Rockford, IL) at a concentration of 1:20,000. Signal detection was performed using ECL chemiluminescent reagent (Super-Signal West Femto Maximum Sensitivity Substrate, Pierce Rockford, IL) and X-ray film.

Image J software was used to measure the band intensities and the percent change was calculated. Relative pixel densities of gel bands were measured using a gel analysis tool in ImageJ software as described (Bhadra and Iovine, 2015). The density of each band was obtained as the area under the curve using the gel analysis tool. For relative density calculation, the density of the Esco2, Cx43, or tubulin bands for the experimental sample was first normalized against the density of the Esco2, Cx43, or tubulin bands from the control sample. Relative pixel density was calculated as the ratio of Esco2 and tubulin or Cx43 and tubulin, where tubulin is the loading control.

Cell Proliferation and Cell Death Assays

For detection of proliferating cells in S-phase, bromodeoxyuridine (5-bromo-2'-deoxyuridine, BrdU) labeling was performed with few modifications (Nechiporuk and Keating, 2002, Iovine et al., 2005). Briefly, 3 dpa MO injected (*esco2*-MO or *esco2*-MM) fish were allowed to swim for 5 min in 50 µg/ml of BrdU (Roche) mixed in system water at 1 dpe/4 dpa and harvested on the same day. The BrdU-labeled fins were fixed in 4% PFA overnight at 4degC and then dehydrated by keeping in 100% methanol overnight. Before use, the fins were rehydrated gradually in a series of methanol solutions containing 0.1% Triton X-100 in PBS (PBTx).

Next, fins were treated for 30 min in a solution containing 2N HCl in PBTx. Following that, the fins were blocked for 2 hr (0.25% bovine serum albumin in PBTx). The primary antibody against BrdU (Roche) is a mouse monoclonal and used at a 1:50 dilution and incubated overnight at 4degC. Extensive washes (4 hr) in the PBTx solution were performed the next day and fins incubated overnight at 4degC in 1:200 dilution of anti-mouse antibody conjugated to Alexa-546 (Invitrogen). The next day extensive washes (4 hr) were performed and the fins mounted in 100% glycerol and visualized under a Nikon Eclipse 80i Microscope equipped with a SPOT-RTKE digital camera (Diagnostic Instruments) and SPOT software (Diagnostic Instruments). For measuring BrdU labeled cells the Image Pro software was used. A ratio of distance migrated by BrdU positive cells from the regenerating tip in μm (a) and the regenerating length in μm (b) was calculated. BrdU labeling was then obtained by measuring a/b ratio of the uninjected and injected (*esco2*-MO and *esco2*-MM) side of the fin.

For both histone-3-phosphate (H3P) and TUNEL assays, 3 dpa MO-injected (*esco2*-MO or *esco2*-MM) fins were harvested at 1 dpe/4 dpa and fixed in 4% PFA overnight at 4degC. These fins were then dehydrated in 100% methanol overnight before use. To detect mitotic cells, H3P staining and the number of H3P positive cells per unit area were carried out as described previously (Ton and Iovine, 2013). The primary and secondary antibodies used for H3P assay are as follows: rabbit anti-histone-3-phosphate (1:200) (anti-H3P, Millipore) and anti-rabbit Alexa 546 (1:200) (Invitrogen). H3P-positive cells were counted without software from within the distal-most 250 μm of the 3rd fin ray as previously established (Iovine et al., 2005; Hoptak-Solga et al., 2008).

TUNEL assay (ApopTag Kit, Chemicon) was performed as described in the manufacturer's instructions with the following modifications. The fins were rehydrated by successive washes in methanol/PBST, treated with proteinase K at a concentration of 5 $\mu\text{g}/\text{ml}$ for 45 min at room temperature, and then re-fixed in 4% PFA in PBS for 20 min. After extensive PBST washes, fins were incubated in ethanol: acetic acid (2:1, v:v) at -20degC for 10 min. Following extensive PBST washes, fins were incubated in equilibrium buffer (from ApopTag Kit) for 1 hr at room temperature, and then incubated overnight in 37degC water bath in TdT solution. The enzymatic reaction was stopped by extensive washes in stop/wash buffer for 3 hr in 37degC water bath, briefly rinsed in PBST and blocked with blocking solution (from ApopTag Kit) for 1 hr. The fins were incubated overnight at 37degC in Rhodamine antibody solution (from ApopTag Kit). Fins were washed extensively in PBST and then mounted in 100% glycerol. Image acquisition was performed using a Nikon Eclipse 80i microscope equipped with a SPOT-RTKE digital camera (Diagnostic Instruments) and SPOT software (Diagnostic Instruments). Cell death was analyzed by counting the number of TUNEL-positive cells without software from the distal-most 250 μm of the 3rd fin ray, similar to the H3P-positive cell counting analysis. For all the experiments at least 6-8 fins were used per trial and at least 3 independent trials were performed. Student's *t*-test ($P < 0.05$) was used for statistical analysis.

qRT-PCR Analysis

The qRT-PCR analysis was completed on total mRNA extracted from 1 dpe/4 dpa harvested fins (3 dpa *esco2*-MO and standard control-MO injected). Total RNA extraction was carried out by

following the standard protocol (Sims et al., 2009). Briefly, Trizol reagent (Gibco) was used to extract mRNA from minimum of 10 fins. For making cDNA, 1 μg of total RNA was reverse transcribed with SuperScript III reverse transcriptase (Invitrogen) using oligo (dT) primers. The following primers (2.5 μM) for *keratin*, *cx43* (Sims et al., 2009), *sema3d* (Ton and Iovine, 2013), *hapln1a* (Govindan and Iovine, 2014), and *mpps1* (Bhadra and Iovine, 2015) were used for qRT-PCR analysis. The primers for *shh* and *spry4* were designed using Primer express software (*shh*: forward primer: 5'-GGCTCATGACACAGAGATGCA-3', reverse primer: 5'-CATTACAGAGATGGCCAGCGA-3' and *spry4*: forward primer: 5'-CGCAACGACCTGTTCATCTGA-3', reverse primer: 5'-GCACTC TTGCATTCGAAAAGCA-3'). Data from three independent *esco2*-knockdown RNA samples were used, with qRT-PCR for each gene performed in duplicate, for comparison between experimental treatments. RNA and subsequent cDNA synthesized from standard control MO injected fins served as the control. The standard control MO does not target any zebrafish genes. Analyses of the samples were done using Rotor-Gene 6000 series software (Corbett Research) and the average cycle number (C_T) determined for each amplicon. *Keratin* was used as a housekeeping gene, and the delta C_T (ΔC_T) values represent expression levels normalized to *keratin* values. $\Delta\Delta C_T$ values represent the relative level of gene expression and the fold difference was determined using the $\Delta\Delta C_T$ method ($2^{-\Delta\Delta C_T}$) as described (Ton and Iovine, 2013). Standard deviation was calculated using the comparative method described in User Bulletin 2 # ABI PRISM 7700 Sequence Detection System (http://www3.appliedbiosystems.com/cms/groups/mcb_support/documents/generaldocuments/cms_040980.pdf).

Heat Shock Induction of cx43 Expression

Tg(hsp70:miR-133sp^{pd48}) are denoted as transgene-positive (Tg+) and their siblings denoted as transgene-negative (Tg-) were used in the heat shock experiment (Yin et al., 2012). For all the experiments at least six to eight fish were used per trial and at least 3 independent trials were performed. *esco2*-knockdown was performed on 3dpa Tg+ and Tg- fish as described above. After 4 hr, both groups were heat shocked at 37°C for 1 hr and returned to the system water for recovery. These groups were then denoted by Tg+HS+ and Tg-HS+, respectively. To confirm that rescue depended on *cx43*, we also examined phenotypes in the transgenic line without heat shock (Tg+HS-). Induction of the transgene expression upon heat shock was confirmed after 24 hr by screening for GFP-positive fins in the Tg+HS+ group. The control groups (Tg-HS+ and Tg+HS-) were negative for GFP expression after heat shock. For measurement of regenerate length and segment length fins were harvested at 4 dpe/7 dpa and calcein stained as previously described (Du et al., 2001; Sims et al., 2009). The measurement and data analysis were done as described below. Image acquisition was carried out by using the Nikon Eclipse 80i microscope equipped with a SPOT-RTKE digital camera (Diagnostic Instruments) and SPOT software (Diagnostic Instruments). Image Pro software was used for regenerate and segment length measurements.

To evaluate the regenerate length and segment length of *Tg(hsp70:miR-133sp^{pd48})* fins, the *esco2*-MO injected side of each fin was compared with its un-injected side by % similarity method as described (Bhadra and Iovine, 2015). Briefly, the length of the injected side and uninjected sides were measured in μm and denoted as A and B respectively. The % similarity for

each fin was calculated by using the formula: $[(A/B) \times 100]$. Values close to 100% indicate that the *esco2*-MO has no effect on the phenotype whereas a value less than 100% indicate that the MO has an effect on the observed phenotype. The mean of % similarity for the *esco2*-knockdown experimental group (Tg+HS+) and the corresponding *esco2*-knockdown control groups (Tg-HS+ and Tg+HS-) were estimated and compared, and the statistical significance between the groups was determined using two tailed unpaired student's *t*-test ($P < 0.05$). Segment length analysis was performed on calcein stained fins. Briefly, for segment length, the distance between the first two newly formed joints following amputation was measured (in the 3rd fin ray from either the dorsal or ventral end) because that was previously established as a standard (Iovine and Johnson, 2000). To evaluate the phenotypic effect of segment length, the % similarity method was used as described above.

Acknowledgments

The authors thank Rebecca Bowman for care of the zebrafish colony, members of the Iovine and Skibbens labs and the Cassbens group for critical discussion, and the Lehigh University Faculty Innovation Grant (FIG) which supported this research.

References

- Barbero JL. 2013. Genetic basis of cohesinopathies. *Appl Clin Genet* 6:15–23.
- Ben-Shahar TR, Heeger S, Lehane C, East P, Flynn H, Skehel M, Uhlmann F. 2008. Eco1- dependent cohesin acetylation during establishment of sister chromatid cohesion. *Science* 321:563–566.
- Bhadra J, Iovine MK. 2015. Hsp47 mediates Cx43-dependent skeletal growth and patterning in the regenerating fin. *Mech Dev* (in press) doi: 10.1016/j.med.2015.06.004.2015.
- Bose T, Lee KK, Lu S, Xu B, Harris B, Slaughter B, Gerton JL. 2012. Cohesin proteins promote ribosomal RNA production and protein translation in yeast and human cells. *PLoS Genet* 8: e1002749.
- Castronovo P, Gervasini C, Cereda A, Masciadri M, Milani D, Russo S, Larizza L. 2009. Premature chromatid separation is not a useful diagnostic marker for Cornelia de Lange syndrome. *Chromosome Res* 17:763–771.
- Choi HK, Kim B J, Seo JH, Kang JS, Cho H, Kim ST. 2010. Cohesin establishment factor, Eco1 represses transcription via association with histone demethylase, LSD1. *Biochem Biophys Res Commun* 394:1063–1068.
- Deardorff MA, Kaur M, Yaeger D, Rampuria A, Korolev S, Pie J, Krantz ID. 2007. Mutations in cohesin complex members SMC3 and SMC1A cause a mild variant of Cornelia de Lange syndrome with predominant mental retardation. *Am J Hum Genet* 80:485–494.
- Deardorff MA, Bando M, Nakato R, Watrin E, Itoh T, Minamino M, Shirahige K. 2012. HDAC8 mutations in Cornelia de Lange syndrome affect the cohesin acetylation cycle. *Nature* 489:313–317.
- Deardorff MA, Wilde JJ, Albrecht M, Dickinson E, Tennstedt S, Braunholz D, Kaiser FJ. 2012. RAD21 mutations cause a human cohesinopathy. *Am J Hum Genet* 90:1014–1027.
- Dorsett D, Merkenschlager M. 2013. Cohesin at active genes: a unifying theme for cohesin and gene expression from model organisms to humans. *Curr Opin Cell Biol* 25:327–333.
- Du SJ, Frenkel V, Kindschi G, Zohar Y. 2001. Visualizing normal and defective bone development in zebrafish embryos using the fluorescent chromophore calcein. *Dev Biol* 238:239–246.
- Ebert MS, Neilson JR, Sharp PA. 2007. MicroRNA sponges: competitive inhibitors of small RNAs in mammalian cells. *Nat Methods* 4:721–726.
- Gard S, Light W, Xiong B, Bose T, McNairn AJ, Harris B, Gerton JL. 2009. Cohesinopathy mutations disrupt the subnuclear organization of chromatin. *J Cell Biol* 187:455–462.
- Gerhart SV, Eble DM, Burger RM, Oline SN, Vacaru A, Sadler KC, Iovine MK. 2012. The Cx43-like connexin protein Cx40. 8 is differentially localized during fin ontogeny and fin regeneration. *PLoS One* 7:e31364–e31364.
- Gerton JL. 2012. Translational mechanisms at work in the cohesinopathies. *Nucleus* 3:520–525.
- Gillis LA, McCallum J, Kaur M, DeScipio C, Yaeger D, Mariani A, Krantz ID. 2004. NIPBL mutational analysis in 120 individuals with Cornelia de Lange syndrome and evaluation of genotype-phenotype correlations. *Am J Hum Genet* 75:610–623.
- Gordillo M, Vega H, Trainer AH, Hou F, Sakai N, Luque R, Jabs EW. 2008. The molecular mechanism underlying Roberts syndrome involves loss of ESCO2 acetyltransferase activity. *Hum Mol Genet* 17:2172–2180.
- Goss RJ, Stagg MW. 1957. The regeneration of fins and fin rays in *fundulus heteroclitus*. *J Exp Zool* 136:487–507.
- Govindan J, Iovine MK. 2014. Hapln1a is required for Connexin43-dependent growth and patterning in the regenerating fin skeleton. *PLoS One* 9:e88574.
- Haas HJ. 1962. Studies on mechanisms of joint and bone formation in the skeleton rays of fish fins. *Dev Biol* 5:1–34.
- Hoptak-Solga AD, Nielsen S, Jain I, Thummel R, Hyde DR, Iovine MK. 2008. Connexin43 (GJA1) is required in the population of dividing cells during fin regeneration. *Dev Biol* 317:541–548.
- Horsfield JA, Print CG, Monnich M. 2012. Diverse developmental disorders from the one ring: distinct molecular pathways underlie the cohesinopathies. *Front Genet* 3:171.
- Iovine MK, Higgins EP, Hindes A, Coblitz B, Johnson SL. 2005. Mutations in connexin43 (GJA1) perturb bone growth in zebrafish fins. *Dev Biol* 278:208–219.
- Iovine MK, Johnson SL. 2000. Genetic analysis of isometric growth control mechanisms in the zebrafish caudal fin. *Genetics* 155: 1321–1329.
- Ivanov D, Schleiffer A, Eisenhaber F, Mechtler K, Haering CH, Nasmyth K. 2002. Eco1 is a novel acetyltransferase that can acetylate proteins involved in cohesion. *Curr Biol* 12:323–328.
- Kawauchi S, Calof AL, Santos R, Lopez-Burks ME, Young CM, Hoang MP, Lander AD. 2009. Multiple organ system defects and transcriptional dysregulation in the *nipbl*(+/-) mouse, a model of Cornelia de Lange syndrome. *PLoS Genet* 5:e1000650.
- Kim BJ, Kang KM, Jung SY, Choi HK, Seo JH, et al. 2008. *Esco2* is a novel corepressor that associates with various chromatin modifying enzymes. *Biochem Biophys Res Commun* 372(2): 298–304.
- Krantz ID, McCallum J, DeScipio C, Kaur M, Gillis LA, Yaeger D, Jackson LG. 2004. Cornelia de Lange syndrome is caused by mutations in NIPBL, the human homolog of *Drosophila melanogaster* Nipped-B. *Nat Genet* 36:631–635.
- Laforest L, Brown CW, Poleo G, Géraudie J, Tada M, Ekker M, Akimenko MA. 1998. Involvement of the sonic hedgehog, patched 1 and *bmp2* genes in patterning of the zebrafish dermal fin rays. *Development* 125(21):4175–4184.
- Lee Y, Grill S, Sanchez A, Murphy-Ryan M, Poss KD. 2005. Fgf signaling instructs position-dependent growth rate during zebrafish fin regeneration. *Development* 132:5173–5183.
- Leem YE, Choi HK, Jung SY, Kim BJ, Lee KY, Yoon K, Kim ST. 2011. *Esco2* promotes neuronal differentiation by repressing Notch signaling. *Cell Signal* 23:1876–1884.
- Liu J, Krantz ID. 2009. Cornelia de Lange syndrome, cohesin, and beyond. *Clin Genet* 76:303–314.
- Loya CM, Lu CS, Van Vactor D, Fulga TA. 2009. Transgenic microRNA inhibition with spatiotemporal specificity in intact organisms. *Nat Methods* 6:897–903.
- Mannini L, Liu J, Krantz ID, Musio A. 2010. Spectrum and consequences of SMC1A mutations: the unexpected involvement of a core component of cohesin in human disease. *Hum Mutat* 31:5–10.
- Mehta GD, Kumar R, Srivastava S, Ghosh SK. 2013. Cohesin: functions beyond sister chromatid cohesion. *FEBS Lett* 587: 2299–2312.
- Monnich M, Kuriger Z, Print CG, Horsfield JA. 2011. A zebrafish model of Roberts syndrome reveals that *Esco2* depletion interferes with development by disrupting the cell cycle. *PLoS One* 6: e20051.

- Morita A, Nakahira K, Hasegawa T, Uchida K, Taniguchi Y, Takeda S, Yanagihara I. 2012. Establishment and characterization of Roberts syndrome and SC phocomelia model medaka (*Oryzias latipes*). *Dev Growth Differ* 54:588–604.
- Musa FU, Ratajczak P, Sahu J, Pentlicky S, Fryer A, Richard G, Willoughby CE. 2009. Ocular manifestations in oculodentodigital dysplasia resulting from a heterozygous missense mutation (L113P) in GJA1 (connexin43). *Eye (Lond)* 23:549–555.
- Musio A, Selicorni A, Focarelli ML, Gervasini C, Milani D, Russo S, Larizza L. 2006. X-linked Cornelia de Lange syndrome owing to SMC1L1 mutations. *Nat Genet* 38:528–530.
- Nechiporuk A, Keating MT. 2002. A proliferation gradient between proximal and msxb-expressing distal blastema directs zebrafish fin regeneration. *Development* 129:2607–2617.
- Paznekas WA, Boyadjiev SA, Shapiro RE, Daniels O, Wollnik B, Keegan CE, Jabs EW. 2003. Connexin 43 (GJA1) mutations cause the pleiotropic phenotype of oculodentodigital dysplasia. *Am J Hum Genet* 72:408–418.
- Poss KD, Nechiporuk A, Hillam AM, Johnson SL, Keating MT. 2002. Mps1 defines a proximal blastemal proliferative compartment essential for zebrafish fin regeneration. *Development* 129:5141–5149.
- Revenkova E, Focarelli ML, Susani L, Paulis M, Bassi MT, Mannini L, Musio A. 2009. Cornelia de Lange syndrome mutations in SMC1A or SMC3 affect binding to DNA. *Hum Mol Genet* 18:418–427.
- Rudra S, Skibbens RV. 2013. Chl1 DNA helicase regulates Scc2 deposition specifically during DNA-replication in. *PLoS One* 8:e75435.
- Schule B, Oviedo A, Johnston K, Pai S, Francke U. 2005. Inactivating mutations in ESCO2 cause SC phocomelia and Roberts syndrome: no phenotype-genotype correlation. *Am J Hum Genet* 77:1117–1128.
- Sims K Jr, Eble DM, Iovine MK. 2009. Connexin43 regulates joint location in zebrafish fins. *Dev Biol* 327:410–418.
- Skibbens RV, Colquhoun JM, Green MJ, Molnar CA, Sin DN, Sullivan BJ, Tanzosh EE. 2013. Cohesinopathies of a feather flock together. *PLoS Genet* 9:e1004036.
- Skibbens RV, Corson LB, Koshland D, Hieter P. 1999. Ctf7p is essential for sister chromatid cohesion and links mitotic chromosome structure to the DNA replication machinery. *Genes Dev* 13:307–319.
- Skibbens RV, Marzillier J, Eastman L. 2010. Cohesins coordinate gene transcriptions of related function within *Saccharomyces cerevisiae*. *Cell Cycle* 9:1601–1606.
- Smith A, Zhang J, Guay D, Quint E, Johnson A, Akimenko MA. 2008. Gene expression analysis on sections of zebrafish regenerating fins reveals limitations in the whole-mount in situ hybridization method. *Dev Dyn* 237:417–425.
- Strom L, Lindroos HB, Shirahige K, Sjogren C. 2004. Postreplicative recruitment of cohesin to double-strand breaks is required for DNA repair. *Mol Cell* 16:1003–1015.
- Terret ME, Sherwood R, Rahman S, Qin J, Jallepalli PV. 2009. Cohesin acetylation speeds the replication fork. *Nature* 462:231–234.
- Thummel R, Bai S, Sarras MP, Song P, McDermott J, Brewer J, Godwin AR. 2006. Inhibition of zebrafish fin regeneration using in vivo electroporation of morpholinos against fgfr1 and msxb. *Dev Dyn* 235:336–346.
- Ton QV, Iovine MK. 2013. Determining how defects in connexin43 cause skeletal disease. *Genesis* 51:75–82.
- Tonkin ET, Wang TJ, Lisgo S, Bamshad MJ, Strachan T. 2004. NIPBL, encoding a homolog of fungal Scc2-type sister chromatid cohesion proteins and fly nipped-B, is mutated in Cornelia de Lange syndrome. *Nat Genet* 36:636–641.
- Toth A, Ciosk R, Uhlmann F, Galova M, Schleiffer A, Nasmyth K. 1999. Yeast cohesin complex requires a conserved protein, Eco1p (Ctf7), to establish cohesion between sister chromatids during DNA replication. *Genes Dev* 13:320–333.
- Unal E, Arbel-Eden A, Sattler U, Shroff R, Lichten M, Haber JE, Koshland D. 2004. DNA damage response pathway uses histone modification to assemble a double-strand break-specific cohesin domain. *Mol Cell* 16:991–1002.
- Unal E, Heidinger-Pauli JM, Kim W, Guacci V, Onn I, Gygi SP, Koshland DE. 2008. A molecular determinant for the establishment of sister chromatid cohesion. *Science* 321:566–569.
- Van der Lelij P, Chrzanowska KH, Godthelp BC, Rooimans MA, Oostra AB, Stumm M, de Winter JP. 2010. Warsaw breakage syndrome, a cohesinopathy associated with mutations in the XPD helicase family member DDX11/ChlR1. *Am J Hum Genet* 86:262–266.
- Vega H, Waisfisz Q, Gordillo M, Sakai N, Yanagihara I, Yamada M, Joenje H. 2005. Roberts syndrome is caused by mutations in ESCO2, a human homolog of yeast ECO1 that is essential for the establishment of sister chromatid cohesion. *Nat Genet* 37:468–470.
- Wei Y, Yu L, Bowen J, Gorovsky MA, Allis CD. 1999. Phosphorylation of histone H3 is required for proper chromosome condensation and segregation. *Cell* 97:99–109.
- Westerfield M. 1993. *The zebrafish book*. Eugene: University of Oregon Press.
- Whelan G, Kreidl E, Wutz G, Egner A, Peters JM, Eichele G. (2012). Cohesin acetyltransferase Escs2 is a cell viability factor and is required for cohesion in pericentric heterochromatin. *EMBO J* 31:71–82.
- Yin VP, Lepilina A, Smith A, Poss KD. 2012. Regulation of zebrafish heart regeneration by miR-133. *Dev Biol* 365:319–327.
- Yuan B, Pehlivan D, Karaca E, Patel N, Charnig WL, Gambin T, Lupski JR. 2015. Global transcriptional disturbances underlie Cornelia de Lange syndrome and related phenotypes. *J Clin Invest* 125:636.
- Zanotti S, Canalis E. 2013. Notch signaling in skeletal health and disease. *Eur J Endocrinol* 168:R95–R103.
- Zhang B, Chang J, Fu M, Huang J, Kashyap R, Salavaggione E, Milbrandt J. 2009. Dosage effects of cohesin regulatory factor PDS5 on mammalian development: implications for cohesinopathies. *PLoS One* 4:e5232.
- Zhang J, Shi X, Li Y, Kim BJ, Jia J, Huang Z, Qin J. 2008. Acetylation of Smc3 by Eco1 is required for S phase sister chromatid cohesion in both human and yeast. *Mol Cell* 31:143–151.